INTERFACE FORCES CALCULATION FOR MULTIPHASE FLOW SIMULATION

Clovis R. Maliska, António F. C. da Silva, Ricardo V.P. Rezende, Ivan C. Georg

Dept. of Mechanical Engineering, Federal University of Santa Catarina – Computational Fluid Dynamics Laboratory – SINMEC, Postal Office Box 476, 88040-900. Florianopolis, SC, Brazil.
maliska@sinmec.ufsc.br

ABSTRACT

Despite the tremendous growth in computational resources, multiphase flows are far from being simulated with generality and accuracy. Keeping track of all interfaces and applying the proper boundary conditions, for example in an industrial gas-liquid flow, is not yet foreseeing possible in a near future, if it will, with the numerical background now available. The growth of the use of simulation tools for multiphase flows rely, therefore, in creating interface models which tries to represent with more fidelity the complex physics happening at the interfaces. This is a research topic which has a very large body of literature available, both on the fundamental physics as well as in theoretical analysis of the forces acting at the interfaces. This paper follows this trend, and an interfacial tracking method (VOF) is used to simulate the behavior of a rising bubble immersed in a quiescent liquid, as well as the buoyancy-driven motion of a viscous drop in a constricted channel. A brief review of the important interfacial forces used in CFD simulations of multiphase flows are discussed. Numerical results are compared with the available experimental data and the interfacial forces calculated from the numerical data are compared with numerical and experimental results. Attention given to the transient behavior of the coefficients normally used in CFD simulations.

1. INTRODUCTION

Multiphase flows are important in most industrial applications including energy conversion, paper manufacturing, medical and nuclear applications. Many combustion and energy systems involve dilute multiphase flow, ranging from droplet sprays in high-speed gas turbine combustor flow to bubbly pipe flows of chemical reactors. A better understanding of the multiphase interactions can lead to increases in performance, reduction in cost and improved safety in several important engineering areas [1]. Up to very recently, the design of equipments involving multiphase flows relied strongly on correlations obtained experimentally. This narrows the range of the design variables. Experimental studies present a number of difficulties because the probes can interfere with the flow and because multiphase systems can be optically opaque. Considerable amount of research has been done in developing measuring systems based on new optical and laser technologies. Moreover, multiphase flows are well known for the difficulties in setting up fully controlled physical experiments. Fine measurements, like the flow inside bubbles, or flows near the bubble surface to investigate the existence of local slip flow are not easy to realize. But the only way for improving the interface models is to set up fine measurements close to the interface.

Computer simulations, in the other hand, permit to include or neglect gravity, account for the effects of the geometrical configuration, process modifications and to perform many others variations in the physical problem. But, the great complexity of scales of the phenomena of practical multiphase flows, with different length and time scales interacting in a broad range is very difficult to model mathematically. One example is the coalescence of drops or bubbles where the interfaces are free to deform and break up. The forces in such systems are very complex, of different types and in the spatial-temporal domain, therefore observed over a large range of length scales [2]. Only recently it has become possible to experimentally observe the rapid motions during the coalescence of two water drops [3].

Generally, the averaged description is used to model multiphase flow in an industrial level, the so-called Eulerian model, where the dispersed phase, like the continuous one, is described as a continuous fluid with appropriate closures (interfacial momentum transfer between the phases, which includes a number of force contributions like viscous drag, added mass and lift, among others). In these models, only the averaged local properties are calculated. The properties of each individual dispersed particle or bubble, can be modeled by the Lagrangian formulation, but unfortunately the amount of particles or bubbles that can be tracked is, even today and in the near future, very limited, [4]. Other method to describe multiphase flow is the interface tracking methods. These methods describe both fluids with one set of equations and solve another equation for the evolution of the interfaces between the fluids.

The closures required in the Eulerian model have to be modeled or provided by empirical data. The problem can be to find closures that are as simple as possible, while incorporating just enough physics to accomplish this, for a given range or phenomena and a specified accuracy. It could be provided by direct numerical experiments. This approach requires transient numerical experiments at the scale of the closure model. One could simulate the motion of one bubble, resolving all scales of the flow and then calculate the forces acting on the bubble. The same procedure can be used for two or three bubbles or for an array of bubbles. The forces are then calculated and the relative importance of them could be determined and compared with empirical data. This procedure is easily controlled, in principle, better than the same experiment, providing better results. However, the difficulty in realizing fine experiments and also to solve numerically the complex multiphase flows, even for few bubbles, hinders the development of general closure models to be used with the two-fluid approach.

In this paper we present a brief review of the important forces entering the interface models for multiphase flow simulation. We also present some numerical results for the buoyancy bubble flow in a straight channel as well as a

upward drop flow in a wavy duct. These are preliminary results of a research project in which the main goal is to obtain more general closure models for CFD calculations. This effort will be supported by fine experimental measurements.

2. BRIEF REWIEW OF THE ACTING FORCES

The ability of a multiphase code to predict the behavior of gas-liquid or gas-solid flow are limited by the closure models used to represent the transfer of quantities between the phases. Researchers in this field have been worked to obtain rational expressions for the forces acting on bubbles (or particles) over the last twenty years [5]. A general transient two-phase flow problem can be formulated by using the well-known two-fluid model, this model, as already pointed-out, depends on the availability of closure models for the interfacial forces. The generalized drag force per unit volume, $\mathbf{M}_{i,d}$, which is a combination of several interfacial forces is given by, (Hibiki and Ishii [6])

$$\begin{aligned}\mathbf{M}_{id} &= \frac{\phi}{V}\left(\mathbf{F}_d^D + \mathbf{F}_d^V + \mathbf{F}_d^B + \mathbf{F}_d^L + \mathbf{F}_d^W + \mathbf{F}_d^T\right) \\ &= \mathbf{M}_d^D + \mathbf{M}_d^V + \mathbf{M}_d^B + \mathbf{M}_d^L + \mathbf{M}_d^W + \mathbf{M}_d^T,\end{aligned} \tag{1}$$

where ϕ, V, **F** and **M** are the volume fraction (or void fraction in a gas-liquid two-phase flow), volume of a typical particle, force, and force per unit of volume respectively. The subscript *d* indicates dispersed phase, and the superscripts of *D*, *V*, *B*, *L*, *W* and *T* mean standard drag, virtual mass, Basset, normal lift, wall lift and turbulent dispersion force of a typical single particle, respectively [6].

The first term on the right-hand side is the force due to viscous and shape effects; the second term is the force required to accelerate a quantity of mass of the surrounding fluid due to the bubble (or particle) motion. The third term, known as the history or Basset force, is the effect of the acceleration on the viscous drag and the boundary-layer development (Basset) [7], or the relative acceleration between the two phases [4]. There is not even full agreement of its formulation and when modeling, this force is almost always neglected. The fourth term is the lift force normal to the relative velocity due to rotation of the fluid (the rotation causes pressure difference normal to the flow [8]). The fifth term is the wall lift force due to the velocity distribution change around particles near a wall, and the last term is the turbulent dispersion force due to the concentration gradient [9], or the effect of turbulence fluctuations on the effective momentum transfer. Because of the very weak relative density of bubbles compared to that of the liquid, almost all the inertia is contained in the liquid, making inertial-induced hydrodynamics forces particularly important in the prediction of bubble motion, [5]. Some difficulties are encountered with bubbly flows; the shapes of the bubbles can change with the local hydrodynamic conditions, adding new degrees of freedom to an already complex problem. Following, a brief description of the acting forces in a bubble/particle are described, trying just to point out the difficulties and uncertainties in modeling them, if they are to be used as closure models for the interfacial problem in CFD simulations.

In fact, there is a single force acting on the interface bubble/liquid, liquid/particle, gas/particle, gas/drop, which is the combination of all effects, the physics of the flow. To split this force in several types was done for engineering convenience only. Therefore, in order to develop new closure models for the interfacial force, it seems that more complex flows, even with a single bubble/particle, need to be solved, generating more general closure models, as done in [30].

Drag Force

Drag force is the result of the viscous effect in the boundary layer and pressure differences caused by the shape of the bubble. Except in low-Reynolds number regime, no theory is generally available for determining the viscous drag experienced by a bluff body [5]. For free liquid contamination, the bubble-liquid interaction seems to escape this rule because the viscosity of the gas filling the bubble is typically much smaller than the viscosity of the surrounding liquid. In this case, there is the possibility of slip along the surface of the bubble and the boundary condition imposed at the bubble surface should be of a zero-shear-stress rather than a no-slip one (Batchelor) [10]. It is not fully determined the influence of this boundary condition on the resulting drag force as a function of the Reynolds number.

For dilute flows, the interphase momentum transfer due to shape and viscous drag is modeled based on the drag on a single particle in an infinite fluid [4], given by

$$\mathbf{F}_\mathrm{d}^\mathrm{D} = \phi_\mathrm{g}\rho_\mathrm{l}\left(\frac{\rho_\mathrm{g}}{\rho_\mathrm{l}}\frac{3}{4}\frac{\mathrm{C_D}}{\mathrm{d_p}}\left|\mathbf{U}_\mathrm{r}\right|\mathbf{U}_\mathrm{r}\right) \tag{2}$$

where, $\mathrm{C_D}$ is the drag coefficient, d_p is the average local particle or equivalent bubble diameter, ϕ_g is the gas volume fraction, ρ_g and ρ_l are the gas and liquid densities and $\mathbf{U_r}$ is the relative local velocity between the fluid and the solid or gas phase.

The drag coefficient for a single-particle system depends not only on the flow regimes but also on the nature of the particles; i.e., solid particles, drop or bubbles. Therefore, for a multiparticle system these differences are also expected to play central roles in determining the drag correlation [11]. At sufficiently low particles Reynolds numbers [12], drops and bubbles are spherical. High viscosity and/or high surface tension keeps fluid particle spherical. In this case, the drag coefficient behaves the same as for solid spherical particles.

Even in the case of a single particle, C_D is a complex function of the Reynolds (*Re*), Eötvös (*Eo*), and Morton (*Mo*) numbers. The shapes of the bubbles vary with size, continuous-flow field, and the physical properties of the system. Clift et at. [13], presented correlations for the terminal velocity of single bubbles in various size ranges. When gas fraction increases, the interaction between bubbles becomes more vigorous. Bubbles collide, they coalesce and break up and affect their neighboring bubbles. Drag formulations for single bubbles cannot be expected to apply in this situation, since the bubbles in this case do not move altogether independently of each other.

Harper [14] observed that bubbles flowing in-line one after the other, moved more rapidly than single bubbles of the same size, as a result of the interaction of the particles with the wake flow, indicating that the correlations to be used in CFD simulation for multiple bubbles needs improvements. Ishii and Zuber [15] made a careful study of the bubble rise velocities in dispersed flow and developed drag formulations

useful for a whole gas fraction range. The actual local gas fraction is a variable in the drag formulation. They cover flow regimes from the Stokes regime through the distorted particle regime and up to the churn turbulent regime. The approach based on experimental data is, apparently, the best-justified way to adjust the generalized drag formulation for high gas concentration. Jakobsen [16] adopted the correlation valid in the churn turbulent regime to model the flow structure in the turbulent bubble column; it was found that the physical effect of this relation was to decrease the relative velocity between the liquid and gas with decreasing the gas fraction, contrary to experimental measurements reported in the literature. This discrepancy clearly indicates that the drag coefficient formulations are not so general even for very similar bubbly flows. The outcome of this brief review shows that it is a challenging task to find correlations for the drag force, such that it represents the complex interfacial phenomena occurring in multiphase flows when several local flow regimes and local bubble sizes are present. The question, already raised in this work, is if one should continue trying to model the drag, and the other forces, in an individual form, since what is required is, in fact, is the global force at the interface.

Virtual Mass Force

Drag force takes into account the interaction between liquid and bubbles in a uniform flow field under non-accelerating conditions. If, however, the bubbles are accelerated relative to the liquid, part of the surrounding liquid has to be accelerated as well. This additional force contribution is called the added mass force or virtual mass force.

The concept of virtual mass force can be understood by considering the change in kinetic energy of the fluid surrounding an accelerating bubble/particle. In potential flow the acceleration induces a resisting force on the sphere equal to one-half the mass of the displaced fluid times the acceleration of the sphere [17]. van Wachem and Almsted [4] give a general equation for this force,

$$\mathbf{F}_{\mathrm{d}}^{\mathrm{V}} = \phi_{\mathrm{g}} \rho_{\mathrm{l}} \mathrm{C}_{\mathrm{VM}} \left(\frac{\mathrm{D}\mathbf{U}_{\mathrm{g}}}{\mathrm{Dt}} - \frac{\mathrm{D}\mathbf{U}_{\mathrm{l}}}{\mathrm{Dt}} \right) \tag{3}$$

in which the virtual mass coefficient, C_{VM}, is a function of the volume fraction.

Maxey and Riley [18] deduced theoretically the virtual mass coefficient for spherical rigid particles in potential flow with a value of C_{VM} =0.5. Cook and Harlow [19] used a value of 0.25 for deformed bubbles in water. Geary and Rice [20] suggested 0.69 for spherical bubbles in water. The gas-fraction dependency of the virtual mass coefficient has been reported by [21] and [22], showing a fall in the coefficient with increasing gas fraction from about 0.5 at low gas fractions to the range 0.01-0.001 at gas fractions around 0.3 to 0.4. Drew and Lahey [9] derived forces on a sphere in inviscid flows. They found the same relationship for the lift force as given by Eq. (3). Rivero et al. [23] used a numerical procedure to separate the history and virtual mass forces from the total unsteady force. Their investigations of oscillatory and uniformly accelerating flows established the inviscid result of C_{VM}, =0.5 to be valid even at moderate Reynolds numbers.

As pointed out in [24], in non-uniform flows, the separation of the virtual mass force is complicated by the fact that the non-uniformity not only induces an inertial force but also modifies the viscous drag as a direct consequence of the changes in the surface vorticity distribution. They performed simulations of straining ambient flows over a solid sphere and a spherical bubble at moderate Reynolds number. Based on the computed pressure drag, they evaluated the virtual mass coefficient for the convective acceleration to be 1/2. For instance, in the case of a growing or collapsing, the bubble experiences a virtual mass force even if the relative velocity does not vary with time [25]. Similarly, when the fluid density varies temporally due to rapid compression or expansion, the time-derivative of ρ contributes to the virtual mass force [26]. This "compressional" force retards the body during fluid compression and accelerates it during fluid expansion.

Geometrically, the virtual mass coefficient is a measure of the bluffness of the body, and its value increases as the body (or bubble) becomes oblate because it accelerates or displaces forward a larger volume of fluid. The virtual mass force plays a central role in bubble hydrodynamics because it is weighted against fluid density and is typically a factor of $(\rho/\rho_b) \sim 10^{-3}$ larger than the rate of change of the bubble momentum [5].

Basset Force

Basset force or history force is a viscous force due to the relative acceleration between the two phases. Most often, this force is ignored in continuum modeling, and there is not even full agreement of its formulation even for the single bubble case [4]. Under steady conditions in a uniform ambient flow, the Basset force becomes zero. Drew and Lahey [27] give an expression for the history force,

$$\mathbf{F}_d^B = \frac{9}{d_p} \phi_l \sqrt{\frac{\rho_l \mu_l}{\pi}} \int_0^t \frac{a(\mathbf{r},t)}{\sqrt{t-\tau}} d\tau \tag{4}$$

where $a(\mathbf{r},t)$ is the acceleration between the phases and the $(t-\tau)^{-1/2}$ is the generally accepted Basset kernel for short times.

Lift Force

Lift force represents the transverse force due to rotational strain, velocity gradients, or the presence of walls. A general equation for the lift force caused by rotational strain is given by

$$\mathbf{F}_{\mathrm{d}}^{\mathrm{L,r}} = \phi_{\mathrm{g}} \rho_{\mathrm{l}} \mathrm{C}_{\mathrm{L,r}} \left(\mathbf{U}_{\mathrm{g}} - \mathbf{U}_{\mathrm{l}} \right) \times \boldsymbol{\omega} \tag{5}$$

and the equation for the lift force caused by velocity gradients is given by

$$\mathbf{F}_d^{L,v} = \phi_g \rho_l C_{L,v} \left(\mathbf{U}_g - \mathbf{U}_l \right) \times \left(\nabla \times \mathbf{U}_l \right) \tag{6}$$

where $C_{L,r}$ and $C_{L,v}$ are the lift force coefficients associated with rotational strain and velocity gradients, respectively. From laminar, inviscid flow, the value of 1/2 can be determined for the lift force coefficient for rotational strain. In literature, a wide range of values can be found for the lift force coefficient, as the above equations originated from inviscid flow around a single sphere. Tomiayama et al. [29] have performed experiments of single bubbles in simple shear flows and have found positive and negative values for the lift

force coefficient, depending upon the specific bubble characteristics.

Dandy and Dwyer [30] computed numerically the three-dimensional flow around a sphere in shear flow from continuity and the Navier-Stokes equations. They examined the two contributions to the lateral force, the viscous and the pressure contribution, respectively. The viscous contribution was always found to be positive. The pressure contribution, however, would change sign over the surface of the sphere and was found to be opposite to the classical Magnus force direction, that is, negative, for most Reynolds numbers and shear rates examined. The total lift was always found to be positive, however.

Bubbles do not always behave as predicted as models for rigid spheres. Kariyasaki [31] studied bubbles, drops, and particles in linear shear flow experimentally and showed that the lift on a deformable particle is opposite to that on a rigid sphere. For Reynolds numbers between 0.01 and 8, the drag coefficient could be estimated by Stokes law, the fluid particles would deform into an airfoil shape.

Tomiyama et al. [32] performed both experiments and numerical simulations of the lateral migration of a bubble in a laminar flow and in a quiescent liquid. They studied the effects of the Eötvös number and liquid volumetric flux on the lateral motion. They found a lateral force due to the wall in the near wall region and a lift force due to circulation around the bubble away from the wall. The latter depends strongly on the Eötvös number. In quiescent liquid, they found that bubbles migrated to the center of the duct and then rose straight. They found that increasing the liquid flux in either direction enhanced the lateral motion and that the lift force was proportional to the liquid flux. For modeling purposes, they used a lift force, Eq. (6). They encountered negative values for lift force coefficients. The explanation for the negative lift force coefficients is the distortion of the bubble shape and the subsequent circulation around the bubble. They therefore conclude that the nature of the force is similar to that of the Magnus force. However, it may just a well be classified as a lift force for induced rotation due to deformation. Bubbles exhibit very different motion depending on whether the bubble deforms or not. A spherical bubble experiences a lift to the right, in accordance with theory for rigid spheres, whereas the deformable bubble takes the shape of an airfoil and moves to the left, for example, experiences a negative lift.

These findings shows again the difficulty in separating the effects in a complex flow, indicating that the determination of more general correlations can be useful for simulating multiphase flows in which the interfaces are not tracked.

Turbulent Dispersion Force

Turbulence, of course, affects the whole flow and, therefore, affects the resulting force at the interface. The dispersed phase can damp the turbulent energy of the flow by means of several effects. The size of the bubbles/droplets, the relative velocity between phases and the turbulence intensity of the continuous phase, are some of the flow characteristics which may affect significantly the resulting force. How to take into account these effects on the closure models is the motivation for large amount of research available in the literature. In order to improve the single-phase models, it can be considered that the movement of the bubbles relative to the liquid phase creates drag work in the liquid phase in addition to liquid shear, Svendsen et al. [33]. An empirical coefficient, C_t denotes the fraction of the bubble-induced drag work creating additional turbulence production in the liquid phase. This parameter generally depends on the bubble size and shape, including turbulent kinetic energy on the length (or time) scales of the bubbles. There is no general agreement in the community about these models. The effect of turbulence on interphase momentum transfer is largely unknown. The Lopez de Bertodano (1991) model

$$\mathbf{F}_d^T = \rho_l C_T k_l \nabla \phi_l \tag{7}$$

is used successfully for air bubbles in water with the turbulent coefficient C_T=0.1 to 0.5, however C_T is not universal, [12].

Clift et al. [13] notes that turbulence generally increases the drag although there is some disagreement among the various studies. Soo [34] asserts that the data predominately shows a decrease in drag coefficient due turbulence. Crowe et al. [35] reviewed a number of studies for turbulence effects on particle drag coefficient and noted a wide variety of results (increases and decreases) over a large range of Reynolds number. Issues, which may be responsible for a lack of consistency, include experimental uncertainty, the turbulent spectrum variations, particle and wall influences. While there are theoretical results, which explain some of these trends for bubble rise velocity decrease, [36], no robust empirical correction can be recommended at this point. Universal models are far from being attained, of course, since all forces, which are usually modeled separately, contain influences from each other. In the case of turbulence, this phenomenon greatly influences the flow, what makes extremely difficult to measure its influence over the whole flow and to separate these influences over each of the forces, like drag, virtual and so on.

In this section, we presented some of the available models for the interphase momentum transfer in multiphase flows, trying to pointing out that much more work is required in order to establish reasonable closure models for CFD simulation of multiphase flows. Certainly, the use of massive numerical simulation for solving complex problems, in which the interfaces can be tracked and its local forces calculated, will greatly help the development of more general closure models. Fine experiments will support the numerical calculation of the interfacial force, a quantity which can not be experimentally measured.

3. INTERFACE TRACKING METHODS

When a sharp interface exists, separating two fluids, difficulties arise to accurately simulate these flows. It can be attributed to the fact that the interface separating the fluids needs to be tracked accurately without introducing excessive computational smearing, the well known numerical diffusion. In the past decade a number of techniques, each with their own particular advantages and disadvantages, Annaland et al. [37], have been developed to simulate complex two fluid flow problems. One of the most well known methods is the volume of fluid (**VOF**) method [38] and [39]. This method uses a color function that indicates the fractional amount of fluid present (the local volume fraction of one of the phases) at a certain position in a determined time. This function is unity in computational cells occupied completely by fluid of one of the phases, and zero in regions occupied completely by the other phase, and a value between these limits in the cells that contain a free surface. In **VOF** algorithm, the color function is discontinuous over the interface; however, in the closely

related level-set algorithm, [40] and [41], this function is continuous. The advantage of the level-set algorithm is the simplicity to compute derivatives of the color function, required to calculate the curvature of the surface. However, in flow fields with appreciable vorticity, or in cases where the interface is significantly deformed, level-set methods suffer from loss of mass [4]. The accuracy of **VOF** methods in calculating the curvature of the interface, by determining the derivative of the color function, is difficult from a numerical point of view.

Marker particle methods, [42] and [43], in which fictitious particles are placed along the interface and used to track the motion of the interface, is a very accurate method, but computationally expensive because the interface is reconstructed from the location of the particles in each iteration. Coalescence and breakup of interfaces is a problem, because some method to model these phenomena needs to be used.

Front tracking methods, [44], make use of markers connected to a set of points to track the interface, whereas a fixed or Eulerian grid is used to solve the Navier-Stokes equations. This method is extremely accurate but complex to implement because dynamic remeshing of the Lagrangian interface mesh is required and mapping of the Lagrangian data onto the Eulerian mesh has to be carried out. A proper sub-grid model is needed to represent the coalescence and break up. Automatic merging of interfaces do not occur in front tracking method.

The interface tracking methods commented above consider two separate, incompressible fluid phases. The two phases are separated by a reconstructed interface, from some color function or another Lagrangian representation of the interface, [4]. Now follows the equation systems used in this work.

The governing conservation equations for unsteady, incompressible, Newtonian flow are given by the continuity equation

$$\nabla \cdot \mathbf{U} = 0, \tag{8}$$

the Navier-Stokes equation

$$\rho \frac{\partial \mathbf{U}}{\partial t} + \rho \nabla (\mathbf{U}\mathbf{U}) = -\nabla P + \nabla \cdot \mathbf{T} + \rho g + \mathbf{S} \tag{9}$$

in which ρ is the density of the local fluid, P the local pressure, **S** the surface tension, **T** the viscous stress tensor, and **U** the velocity field. The velocity field holds both the liquid and the gas velocity. Viscosity and density are assumed constant in each of the phases, but may vary.

Standard **VOF** and level set methods make use of a transport equation to determine the evolution of the color function

$$\frac{\partial \phi}{\partial t} + \mathbf{U} \cdot \nabla \phi = 0, \tag{10}$$

where ϕ is the color function, representing the liquid or gas phase.

The surface tension**,** **S**, is included in Eq. (9) as a body force and acts only on the inter-phase boundary surface

$$\mathbf{S} = \gamma \kappa(\mathbf{x}) \nabla \phi, \tag{11}$$

where γ is the surface tension coefficient and κ is the surface curvature given by

$$\kappa = -\nabla \cdot \mathbf{n}, \quad \mathbf{n} = \frac{\nabla \phi}{|\nabla \phi|}. \tag{12}$$

In this work the color function is made equal to volume fraction of surrounding fluid.

In the next section, we present some numerical results using the **VOF** method described above. The idea is to evaluate the model as a tool for the solution of more complex flows for the sake of improving the closure methods for interfacial forces.

4. NUMERICAL RESULTS

To apply the **VOF** method to calculate the interfacial forces in a two-phase problem two physical situations involving a gas bubble moving in an incompressible quiescent liquid is considered. The problems are solved in a 2D Cartesian domain, therefore, the shape of the bubbles differs considerably from their original forms, since one is considering a planar 2D problem. Full 3D and 2D axi-symmetric solutions are being computed for future comparisons.

The first test is based on experimental results performed by [45] for single gas bubbles rising in a liquid. The second test problem, the buoyancy-driven viscous drop in constricted capillaries [46] has numerical and experimental results for comparison.

The two-dimensional numerical simulations were carried out using the CFD code ANSYS CFX release 11^{TM}, which use an element-based finite volume method. All simulations are performed using high-resolution scheme for space discretization and a second order backward difference scheme for the time.

Gas Bubble Moving in a Quiescent Liquid

Bhaga and Weber [45] studied experimentally the rising bubble in a quiescent liquid. They presented experimental results for a wide range of flow regimes. In our numerical experiment, it is used one of the results presented in [45] to compare the shapes, upward velocity and drag correlation. The lift and virtual mass forces are calculated and compared with the numerical and experimental results. The usual dimensionless parameters employed are the Reynolds, Eötvös and Morton numbers defined as

$$\mathrm{Re} = \frac{\rho_f d_e U_t}{\mu_f}; \ \mathrm{Mo} = \frac{g \mu_f^4}{\gamma \rho_f}; \ \mathrm{Eo} = \frac{g d_e^2 \rho_f}{\gamma}; \tag{13}$$

where U_t is the terminal velocity, γ is the surface tension coefficient, d_e is the equivalent diameter of the bubble, ρ_f is the liquid density and μ_f the viscosity of the liquid. It was used the same values of the experimental test for these numbers, (Re=7.16, Mo=41.1 and Eo=116) in the numerical simulations. The physical properties used are shown in Tab. 1.

Table 1. Physical properties.

ρ_f	ρ_f	μ_f	U_t	γ	d_e

1314 kg/m^3	1.185 kg/m^3	12.53 g/cm s	26.16 cm/s	76.9 dynes/cm	2.61 cm

A Cartesian computational grid (801x801) was used in a 20x20 cm domain that gives a grid size of 0.025 cm. The time step used in the simulations was of the order of 10^{-4} second. A circular bubble was inserted in the bottom of the channel filled with liquid at rest and no-slip boundary condition was used for the walls. In Fig. 1 the experimental and numerical shapes of the bubble at terminal velocity is compared. It can be seen that a good qualitative agreement was obtained for the general shape of the bubble.

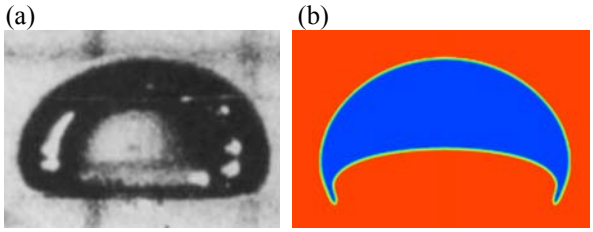

Figure 1. (a) Experimental, from [45] and (b) numerical obtained in this work.

Significant for the purpose of this work is to observe that the interface is well represented, with almost no smearing, what is very common when numerical results using **VOF** methods are calculated. This indicates that grid resolution used is fine enough for representing the interfacial shape of the bubble. It also important to remember that in transient flows, if the interface is not well captured, the errors accumulated along time, being difficult to predict the right shape of the bubble.

The rise velocity of the bubble, V_b, is defined as its baricentric velocity in the vertical direction, by

$$V_b = \frac{\int_V U_g . e_z dV}{\int_V \phi_g dV} \qquad (14)$$

where U_g is the velocity of the gas phase in the vertical direction and ϕ_g is the volume fraction of the gas phase.

Time evolution of the bubble rise velocity is shown in Fig. 2 with the shapes of the bubble indicated. The bubble reaches its terminal velocity at about 0.3 second from the start. Experimental terminal velocity for this case is reported as 0.2616 m/s and the numerical result obtained was 0.243 m/s, with a relative error of about seven per cent. Most probably, this difference is an effect of the wall boundary condition, since the simplifications done in considering a 2D planar flow would increase even more this velocity. More tests with a wider channel and considering 3D flow need to be conducted in order to confirm this.

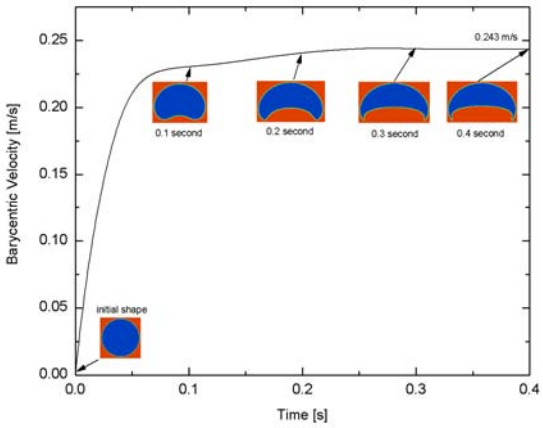

Figure 2. Evolution of the bubble rise velocity with its shape for 5 vertical positions.

The magnitude of the local velocity of the gas flow can be observed in Figs 3 and 4, where it is shown, respectively, the contours of the horizontal and vertical velocity component. The symmetry of the flow inside the bubble can be identified in these two figures. At the upper region of the bubble, the velocity is greater than in the bottom region.

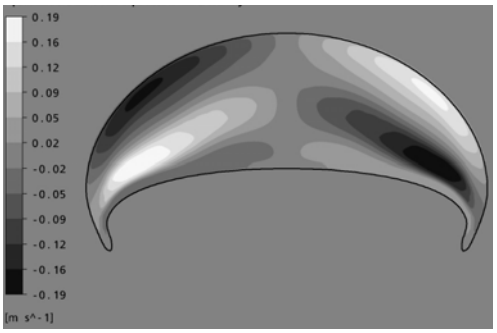

Figure 3. Contours of gas velocity inside the bubble at the terminal velocity (horizontal component)

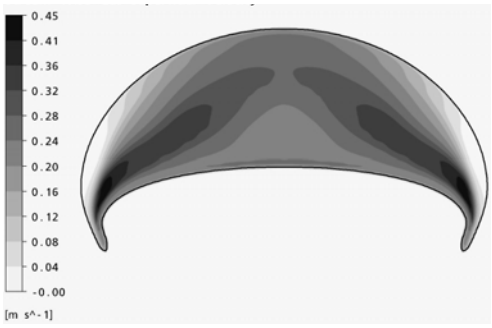

Figure 4. Contours of gas velocity bubble at the terminal velocity (vertical component).

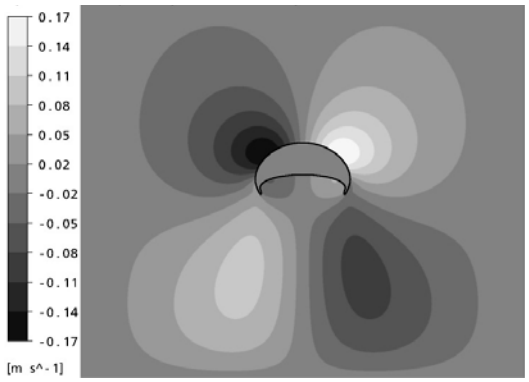

Figure 5. Induced liquid velocity contours at the terminal velocity (horizontal component)

In Figs. 5 and 6 contours of the horizontal and vertical components of the induced liquid velocity is shown. The figure shows a symmetric field with opposite signal for the x-component of the liquid velocity, as expected. Near the bottom of the domain the contours appears deformed, what demonstrates the influence of the boundary of the domain on the results. This is not critical, since velocities in that region are very small. By their turn, lateral walls do not show this behavior.

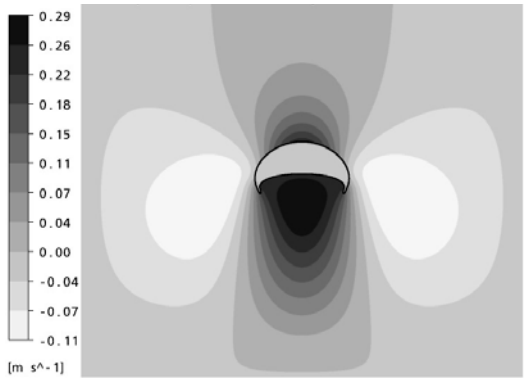

Figure 6. Induced liquid velocity contours at terminal velocity (vertical component)

The drag and lift forces, F_D and F_L, are the components of the fluid force acting on the bubble surface in the transversal and in the streamwise direction, and they can be calculated by the sum of the pressure and viscous contributions, by

$$F_i = F_{ip} + F_{iv} = -\int_S p\mathbf{e}_i \cdot \mathbf{n} dS + \int_S \mathbf{n} \cdot \tau \cdot \mathbf{e}_i dS. \quad (15)$$

The drag and lift coefficients, C_D and C_L, are defined by

$$C_i = \frac{F_i}{0.5\rho_L U_t^2 \pi (\frac{d_e}{2})^2}. \quad (16)$$

in which F_i is the force component acting in the bubble surface in the streamwise and transversal directions already integrated in the bubble surface, and U_t is the terminal velocity calculated numerically. The forces were integrated in the surface using the output from the simulator.

Virtual mass force, by its turn, appears when the flow is accelerating. A balance between buoyancy and virtual mass forces gives

$$C_{vm} = -\frac{\rho_g}{\rho_L} + \frac{(\rho_L - \rho_g)|g|}{\rho_L \frac{dU_{rel}}{dt}} \quad (17)$$

in which the total derivative is defined by

$$\frac{dU_{rel}}{dt} = \frac{\partial \mathbf{U}_g}{\partial t} + \mathbf{U}_g \cdot \nabla \mathbf{U}_g - \frac{\partial \mathbf{U}_L}{\partial t} - \mathbf{U}_L \cdot \nabla \mathbf{U}_L. \quad (18)$$

In Eq. (18) the baricentric velocities are considered. It was observed that, for this case, the spatial derivatives in Eq. (18) plays a minor role in the value of the acceleration. Bhaga and Weber [45] provided experimental results for the drag coefficients. The numerical results of this work for C_D and C_{VM} are compared in Tab. 2.

Table 2. C_D and C_{VM} compared with experimental (C_D) and the expected value of C_{VM} for the flow over a cylinder

	C_D	C_{VM}
Experimental	5.29[45]	
Numerical	5.76	1.35

The numerical result for C_D is closer to the experimental one considering the simplifications adopted. C_L, by its turn, was found to be equal to zero, as expected, since the flow is symmetric. C_{VM}, by its turn shows considerable discrepancy when compared with the value of unity for a 2D cylinder [47]. Some new tests are being conducted in order to clarify this.

Drop buoyancy-driven motion in a constricted capillary

The motion of deformable drops and bubbles through constant and variable cross-section channels are of fundamental importance as a prototype problem in many engineering and scientific applications [46].

In constricted channels, flow is inherently unsteady and inertial effects might be important, especially in the case of small capillary numbers or severely constricted channels. In this work qualitative and quantitative comparisons is realized with the results reported in [46]. These authors used a finite volume front tracking method to simulate a buoyancy-driven motion of drops in constricted channels. Both, numerical and experimental results are reported in [46].

The case studied herein is the flow of a drop with radius R_d= 2.7 mm in a tube with capillary radius R_c=5.00 mm. The non-dimensional drop radius k is defined as the ratio of the equivalent spherical drop radius to the average channel radius k=(R_d/R_c). The value used for k is 0.55. The amplitude of restricted channel used in this work is α=0.28 and the Bond number, Bo=12.91. The physical properties are presented in Tab. 3.

Table 3. Physical properties.

ρ_{drop}	ρ_L	μ_{drop}	μ_L	γ	H*
950 kg/m^3	1.250 kg/m^3	97 mPa.s	450 mPa.s	0.0057 N/m	70 mm

*Channel height

The simulation was performed using the **VOF** method described above with a computational grid of 121x901 volumes (Δy~0.077 mm and Δx~0.097 mm). Figure 7 illustrate a detail on the throat of the mesh used. As shown in the figure, the refinement was concentrated at the central region of the channel.

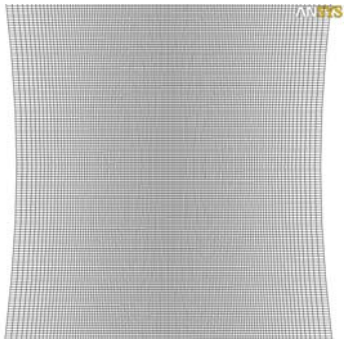

Figure 7. Mesh detail on the throat of the channel.

A qualitative comparison with the experimental drop shape is shown in Fig. 8. As can be seen in this figure, the computed drop shape compares well with the experimental results, indicating the accuracy of the present simulation and the capability of **VOF** method to represent the interfacial shape of the drop. It should me mentioned that the numerical result presented in the left side of Fig. 8 was obtained with a channel where the amplitude of the wavy wall is a little larger than the one used in the experimental work.

Quantitative comparison with the numerical results, reported in [46] for the shape of the drop is shown in Fig 9. This figure shows that the **VOF** method used in this work compares very well with the numerical result (front tracking) reported for the shape of the drop.

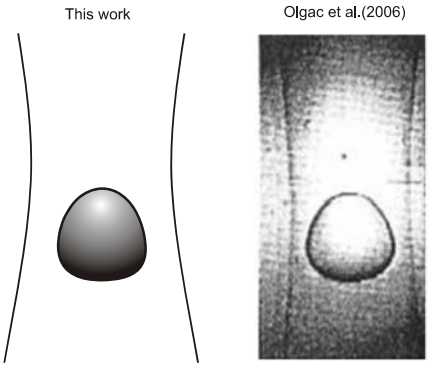

Figure 8. Qualitative comparison between the numerical and experimental shapes of the drop before entering the throat. Extracted from [46].

The rise velocity of the drop was calculated by Eq. 14 and the profile shown in Fig. 10. This figure shows the drop baricentric velocity and the shapes along the capillary tube. There is a sudden acceleration just after the drop is released, demonstrating that the inertia effects are very small. Following, there is a smooth damping of velocity before the throat and after the throat the drop starts to accelerate smoothly again. Inside the throat, there is a modification of the drop shape, with elongation in the streamwise direction. One can note an almost symmetric behavior of the baricentric velocity profile before and after the throat.

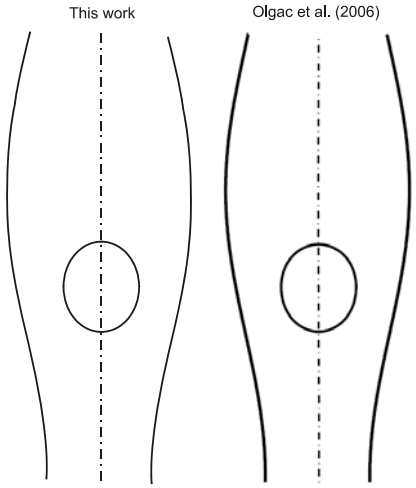

Figure 9. Comparison of the drop shape between the numerical results after the throat, reported by Olgac et al (2006) and the present work.

Drag force and virtual mass are calculated for this numerical result using Eqs. 15 to 18. A comparison is made for drag coefficient and presented in Fig. 11, where the time evolution of C_D is shown. At a low particle Reynolds numbers, the drag coefficient for flows past spherical particles may be computed by

$$C_D = \frac{24}{\mathrm{Re}}, \tag{19}$$

For sphere and also for distorted particles the drag coefficient can be calculated, using an equivalent diameter, by

$$C_D = \frac{4}{3}\frac{g d_e \Delta\rho}{V_b^2 \rho_L}. \tag{20}$$

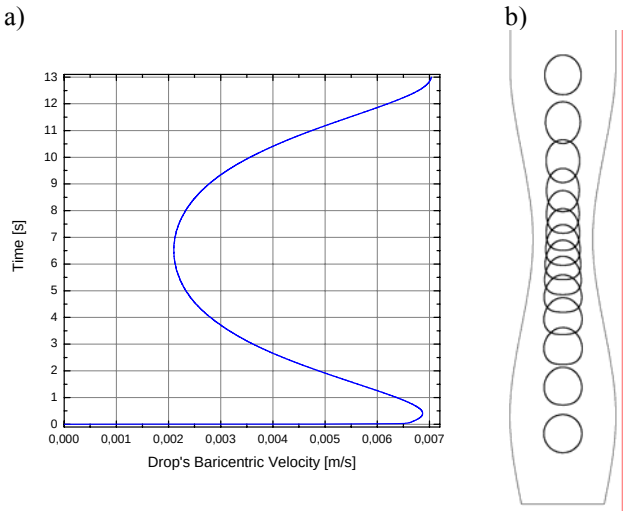

Figure 10. a) Baricentric velocity of the drop; b) Drop's path and its shapes along the wavy channel.

In Fig 11 it is depicted the unsteady C_D coefficient. Three different ways in calculating the drag coefficient were used. The first one uses Eq. (16) in which the force is calculated

through the calculation of the acceleration and the mass involved. The acceleration was calculated using the velocities obtained as output, and Eq. (18). The mass was computed using the density and the volume of the drop considering it as a sphere, even though the flow was considered planar. Eq. (20), by its turn, is obtained from a force balance between buoyancy and drag valid, therefore, for steady state flow. In Fig. 11 Eq. (20) is plotted using as terminal velocity the instantaneously velocity of the rising drop. As can be seen, Eq (16), also considering the terminal velocity as the instantaneous velocity, is in excellent agreement with Eq. (20), what demonstrates that the transient flow of the drop along the wavy channel behaves as a sequence of several steady-state flows. This is a very important finding, since it allows the use of the correlation for steady state flow in transient regime.

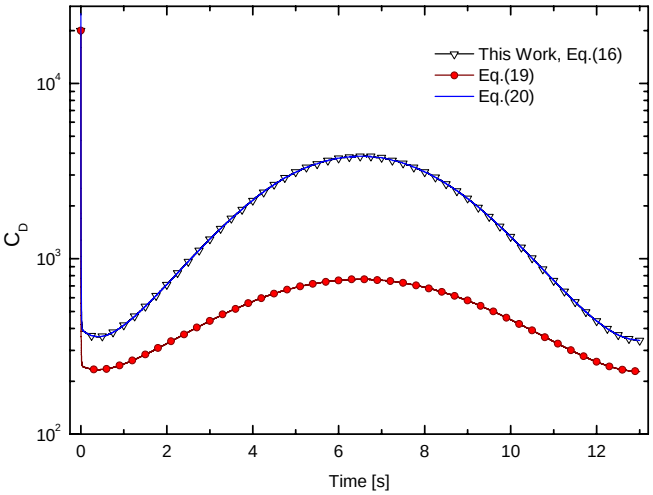

Figure 11. Time evolution of the drag coefficient calculated for this work for sphere (Eq. 19) and for an ellipsoidal shape (Eq. 20).

5. CONCLUSIONS

This work presented a numerical calculation of forces acting on the interface of two fluids considering transient effects. The results are preliminary, and are embodied in a more general research goal of developing closure models to be used in CFD simulations. The main objective is to solve complex 3D problems with several effects involved, seeking for more general closure models, trying to avoid the modeling through the split of the interfacial forces in many types, like drag, lift, virtual mass, among others. With this in mind, a brief overview of the important interfacial forces was described.

The **VOF** method was used for solving the two test problems, namely the flow of a gas bubble rising in a quiescent liquid and the rising drop in a wavy channel. Shapes of the bubble in its terminal velocity were compared with the experimental results reported in [45]. Drag, lift and virtual mass coefficients were calculated by integrating the tangential and normal forces on the surface of the bubble. The expected virtual mass coefficient for the flow over a cylinder does not match with the present results, probably because the non-slip boundary condition used on the walls and the initial boundary condition affect the flow behavior. The consideration of planar flow may have contributed, and this result needs to be analized in more detail.

A fundamental problem, the motion of drops in constricted channels was also solved. Very good agreement with experimental shapes of the drop was obtained. The calculated drag coefficient with the drag correlation used for drops with non-spherical shape agrees well with numerical results. It was demonstrated that the unsteady rising of the drop in the wavy channel is equivalent of a sequence of several steady-state regimes. This is supported by the fact that the unsteady drag agrees very well with the steady drag calculation when the steady-state velocity is substituted by the instantaneous velocity.

In general, the **VOF** method used to simulate realistic physical problems gives good results and can be used as a tool to calculate the interfacial forces in multiphase flows. The accuracy of force calculations will depend on the grid and on temporal refinement, as well as on the order of the numerical scheme. The numerical results shown were solved with a spatial and temporal refinement that resolves much of the flow scales.

ACKNOWLEDGEMENTS

The authors gratefully acknowledge the financial support for this work by CNPq – Conselho Nacional de Desenvolvimento Científico e Tecnológico - through a scholarship for Ivan C. Georg.

REFERÊNCIAS

[1] S. Sundaresan, Modeling the hydrodynamics of multiphase flow reactor: current status and challenges, *AIChE Journal*, vol. 46, n. 6, pp. 1102-1105, 2000.

[2] T.J. Hanratty, T. Theofanous, J-M. Delhaye, J. Eaton, J. McLaughlin, A. Prosperetti, S. Sundaresan, G. Tryggvason, Workshop Findings, *International Journal fo Multiphase Flow*, vol. 9, pp. 1047-1059, 2003.

[3] A. Menchaca-Rocha, A. Martinez-Davalos, R. Nunez, S. Popinet, S. Zaleski, Coalescence of liquid drops by surface tension, *Phys. Rev. E*, n. 4, 046309, 2001.

[4] B.G.M. van Wachem, A.E. Almstedt, Methods for multiphase computational fluid dynamics, *Chemical Engineering Journal*, vol. 96, pp. 81-98, 2003.

[5] J. Magnaudet and I. Eames, The motion of high-Reynolds-number bubbles in inhomogeneous flows, *Annu. Rev. Fluid Mech.*, n. 32, pp. 659-708, 2000.

[6] T. Hibiki, M. Ishii, Lift force in bubbly flow systems, *Chemical Engineering Journal*, vol. 62, pp. 6457-6474, 2007.

[7] A.B. Basset, *A Treatise on Hydrodynamics,Worshop Findings*, vol. 2, Deighton, Bell, Cambridges, (Dover, New York, 1961), 1888.

[8] H. Enwald, E. Peirano, A.-E. Almstedt, Eulerian two-phase flow theory applied to fluidization, *International Journal fo Multiphase Flow*, vol. 22 Suppl., pp. 21-66, 1996.

[9] D.A. Drew, R.T. Jr. Lahey, The virtual mass and lift force on a sphere in rotating and straining inviscid flow, *International Journal fo Multiphase Flow*, vol. 13, pp. 113-121, 1987.

[10] G.K. Batchelor, *An Introduction to Fluid Dynamics*, Cambridge University Press, New Delhi, 1997.

[11] M. Ishii and K. Mishima, Two-fluid model and hydrodynamic constitutive relations, *Nuclear Engineering and Design*, vol.82, pp. 107-126, 1984.

[12] A.D. Burns, Computational fluid dynamics modeling of multiphase flows. Alpha Beta Numerics, Fulwood, Preston, PR28At, UK, 2003.
[13] R. Clift, J.R. Grace and M.E.Weber, *Bubbles, drops and particles,* Academic Press, New York, 1978.
[14] J.F. Harper, The motion of bubbles and drops through liquids, *Adv. Appl. Mech.*, n. 12, pp. 59-129, 1972.
[15] M. Ishii, N. Zuber, Drag coefficient and relative velocity in bubbly, droplet or particulate flows, *AIChE Journal*, vol. 25, pp. 843-855, 1979.
[16] H.A. Jakobsen, On the modelling and simulation of bubble column reactors using two-fluid model, Dr. Ing. Thesis 97, NTH, Trondheim, 1993.
[17] J.B. Joshi, Computational flow modeling and design of bubble column reactors, *Chemical Engineering Journal*, vol. 56, pp. 5893-5933, 2001.
[18] M.R. Maxey and J.J.Riley, Equation of motion for a small sphere in a non-uniform flow, *Phys. Fluids*, vol. 26, pp. 883-889, 1993.
[19] T.L. Cook and F.H. Harlow, Vortices in bubby two phase flow, *International Journal of Multiphase Flow*, vol. 12, pp. 35-61, 1986.
[20] N.W. Geary, R.G. Rice, Circulation in bubble columns: corrections for distorted bubble shape, *American Institute of Chemical Engineering Technology*, vol. 37, n. 10, pp. 1593-1594, 1986.
[21] L. van Wijngaarden, Hydrodinamic iteraction between gas bubbles in liquid, *Journal of Fluid Mechanics*, vol. 77, pp. 27-44, 1976.
[22] Yu.G. Mokeyev, Effect of particle concentration on their drag and induced mass, *Fluid. Mech. Sov. Res.*, vol. 6, pp. 161, 1977.
[23] M. Rivero, Etude par simulaton nuérique des forces exercées sur une inclusion sphérique par un écoulement accéléré, PhD thesis. Inst. Nat. Polytech. Toulose, Toulose, France, 1991.
[24] M. Rivero, J. Magnaudet, J. Fabre, Quelques resultants nouveaux concernat les forces exercées sur une inclusion sphérique par4 un écoulement accéléré, *C. R. Acad. Sci. Paris Série II*, n. 312, pp. 1499-1506, 1991.
[25] D. Lhuillier, Forces d'inertie sur une bulle en expansion se déplaçant dans un fluide, *C. R. Acad. Sci. Paris Série II*, n. 295, pp. 95-98, 1982.
[26] I. Eames, J.C.R. Hunt, Inviscid flow around bodies moving in a weak density gradient in the absence of buoyancy effects, *Journal of Fluid Mechanics*, vol. 353, pp. 331-355, 1997.
[27] D. Drew, R. Lahey, *Particulate two-phase flow,* Butterworth-Heinemann, Boston, Chapter 16, pp. 509-566, 1993.
[28] P. Bagchi and S. Balachandar, Inertial and viscous forces on a rigid sphere in straining flows at moderate Reynolds numbers, *Journal of Fluid Mechanics*, vol. 481, pp. 105-148, 2003.
[29] A. Tomiyama, H. Tamai, I. Zun, S. Hosokawa, Transverse migration of single bubbles in simple shear flows, *Chemical Engineering Science*, vol. 57, pp. 1849-1858, 2002.
[30] D.S. Dandy, H.A. Dwyer, A sphere in shear flow at finite Reynolds number: effect of shear on particle lift, drag, and heat transfer, *Journal of Fluid Mechanics*, vol. 216, pp. 381-410, 1990.
[31] A. Kariyasaki, Behavior of a single gas bubble in a liquid flow with a linear velocity profile, *Proceedings of the 1987 ASME/JSME Thermal Engineering Conference,* n. 384, pp. 261-267, 1987.
[32] A. Tomiyama, A. Sou, A. Zun, I. Kanami, T. Sakaguchi, Effects of Eötvös number and dimensionless liquid volumetric flux on lateral motion of a bubble in a laminar duct flow. *Advances in Multiphase Flow,* Elsevier, pp. 3-15, 1995.
[33] H. Svendsen, H.A. Jakobsen, R. Torvik, Local flow structures in internal loop and bubble column reactors, *Chemical Engineering Science*, vol. 47, pp. 3297-3304, 1992.
[34] S.L. Soo, *Multiphase fluid dynamics,* Aldershot-Brookfield, USA: Gower Technical, 1990.
[35] C.T. Crowe, M. Sommerfeld, Y. Tsuji, *Multiphase flows with droplets and particles,* CRC Press, New York, 1998.
[36] R.E.G. Poorte, On the motion of bubbles in active grid generated turbulent flows, PhD thesis, University of Twenty, Netherlands, September, 1988.
[37] M. van Sint Annaland, N.G. Deen, J.A.M. Kuipers, Numerical simulation of gas bubbles behavior using a tree-dimensional volume of fluid method, *Chemical Engineering Science*, vol. 60, pp. 2999-3011, 2005.
32, pp. 1055-1071, 2006.
[38] C.W. Hirt, B.D. Nichols, Volume of fluid (VOF) method for the dynamics of free boundaries, *Journal of Computational Physics*, vol. 39, p. 201, 1981.
[39] S. Popinet, S. Zaleski, A front-tracking algorithm for accurate representation of surface tension, *International Journal of Numerical Methods in Fluids*, vol. 30, pp. 775-793, 1999.
[40] M. Sussman, P. Smereka, S. Osher, A level set approach for computing solutions to incompressible two-phase flow, *Journal of Computational Physics,* vol. 114, pp. 146-159, 1994.
[41] M. Sussman, E. Fatemi, An efficient interface-preserving level set redistancing algorithm and its application to interfacial incompressible fluid flow, *SIAM Journal of Scientific Computing,* vol. 20, pp. 1165-1191, 1999.
[42] J.E. Welch, F.H. Harlow, J.P. Shannon, B.J. Daly, The MAC method: a computing technique for solving viscous incompressible transient fluid flow problems involving free surfaces. Los Alamos Scientific Laboratory Report LA-3425, 1965.
[43] W.J. Rider, D.B. Kothe, Reconstructing volume tracking, *Journal of Computational Physics,* vol. 141, pp. 112-152, 1998.
[44] S.O. Unverdi, G. Tryggvason, A front tracking method for viscous, incompressible multi-fluid flows, *Journal of Computational Physics,* vol. 100, pp. 25-37, 1992.
[45] D. Bhaga and M.E. Weber, Bubbles in viscous liquids: shapes, wakes and velocities, *Journal of Fluid Mechanics*, vol. 105, pp. 61-85, 1981.
[46] U. Olgac, A.D. Kayaalp, M. Muradoglu, Buoyancy-driven motion and breakup of viscous drops in constricted capillaries, *Journal of Multiphase Flow*, vol.
[47] W. Dijkhuizen, E.I.V. van den Hengel, N.G Deen, M. van Sint Annaland, J.A.M. Kuipers, Numerical investigation of closures for interface forces acting on single air-bubbles in water using Volume of Fluid and Front Tracking models, *Chemical Engineering Science,* n. 60, pp. 6169-6175, 2005.